COMMUNICATION

Cross-Stacking Aligned Carbon-Nanotube Films to Tune Microwave Absorption Frequencies and Increase Absorption Intensities

Hao Sun, Renchao Che, Xiao You, Yishu Jiang, Zhibin Yang, Jue Deng, Longbin Qiu, and Huisheng Peng**

It is well recognized that effective frequency regulation is crucial while challenging for the practical applications of microwave absorption materials.[1–3] For accurate electronic instruments, the shielding frequency needs to be tunable when the frequency of the outer microwave changes. Microwaves with different frequencies are used to detect targeting objects in military applications, so it is necessary to realize the frequency regulation for absorption materials. Although wide and intense investigations have been made, changing the coating thickness of the absorber is still the only available way to tune the microwave absorption frequency according to the transmission line theory. The reflection loss (RL) value is calculated by the following equations.[4,5]

$$RL(\mathrm{dB}) = -20\log_{10}\left|(Z_{\mathrm{in}}-1)/(Z_{\mathrm{in}}+1)\right| \quad (1)$$

$$Z_{\mathrm{in}} = \sqrt{\mu_{\mathrm{r}}/\varepsilon_{\mathrm{r}}}\tanh\left[-j(2\pi fd/c)\sqrt{\mu_{\mathrm{r}}/\varepsilon_{\mathrm{r}}}\right] \quad (2)$$

where ε_r, μ_r, c, f, d and Z_{in} correspond to the relative complex permittivity, permeability, velocity of light, microwave frequency in free space, coating thickness and input impedance of the absorber, respectively. For a certain material with fixed ε_r, μ_r and constant Z_{in}, the absorption frequency f is inversely proportional to the coating thickness of the absorber layer. However, it is inconvenient or even unavailable to change the coating thickness of the absorber in practical applications. For instance, stealth aircraft and warships are designed to absorb microwaves at certain frequency, but the coating thickness has to be changed for another microwave frequency beyond the designed bandwidth, which cannot be done in practice. In addition, the coating thickness is limited by the required light weight of the absorber layer to guarantee the necessary high load and speed. To this end, developing new method to tune the microwave absorption frequency is in great emergency in the area of microwave absorption.

A wide variety of inorganic and organic materials have been extensively explored for microwave absorption materials,[6–12] and carbon nanotubes (CNTs) represent one of the most studied systems due to the combined light weight and remarkable mechanical and electronic properties.[2,5,13–15] The CNTs are generally incorporated into polymers to produce composite microwave absorbers.[7] However, they display reflection losses typically lower than –23 dB (Table S1, Supporting Information). It is well recognized that, for conductive fillers, the electrical conductivities can be greatly enhanced for strong microwave absorptions beyond their percolation thresholds.[15] However, the aggregation of CNTs and difficulty of realizing high contents in polymer matrices prevent the formation of effective networks. It remains challenging to achieve the percolation threshold, thus resulting in poor microwave absorptions.[1,15] To this end, the alignment of CNTs may provide a general and efficient solution. In fact, aligned CNT materials have been widely investigated to produce high-performance solar cells,[16,17] lithium-ion batteries,[18–20] electrochemical supercapacitors[21–23] and various sensors.[24–26]

Herein, aligned CNT sheets are used as building blocks to prepare microwave absorption materials, and the absorption frequency can be accurately controlled by stacking them with different intersectional angles. A remarkable reflection loss of –47.66 dB is achieved by stacking four aligned CNT sheets with an intersectional angle of 90° between two neighboring ones. The incorporation of metal and conducting polymer has further greatly enhanced the microwave-absorption capability. These aligned CNT sheet-based films are particularly promising for lightweight microwave absorption materials.

Vertically aligned CNT arrays were firstly synthesized through a chemical vapor deposition method (Figure S1, Supporting Information) and then pressed down to form the desired CNT films by a smooth polytetrafluoroethylene roller. The CNTs showed a multiwalled structure with an average diameter of ca. 11 nm. The resulting aligned CNT film was lightweight with a low area density of 1.97 g m^{-2} and can be supported by a blade of grass (**Figure 1**a). The thickness of the aligned CNT film was ca. 80 μm. Two aligned CNT films were stacked together with increasing intersectional angles of 0, 15°, 30°, 45°, 60°, 75° and 90°. Figure 1b shows a photograph of two aligned CNT films with an intersectional angle of 45°, and the aligned directions of CNT films were clearly verified by scanning electron microscopy (SEM)

H. Sun, X. You, Y. Jiang, Z, Yang, J. Deng, L. Qiu, Prof. H. Peng
State Key Laboratory of Molecular Engineering of Polymers
Department of Macromolecular Science and Laboratory of Advanced Materials
Fudan University
Shanghai 200438, China
E-mail: penghs@fudan.edu.cn
Prof. R. Che
Department of Materials Science and Laboratory of Advanced Materials
Fudan University
Shanghai 200433, China
E-mail: rcche@fudan.edu.cn

DOI: 10.1002/adma.201403735

COMMUNICATION

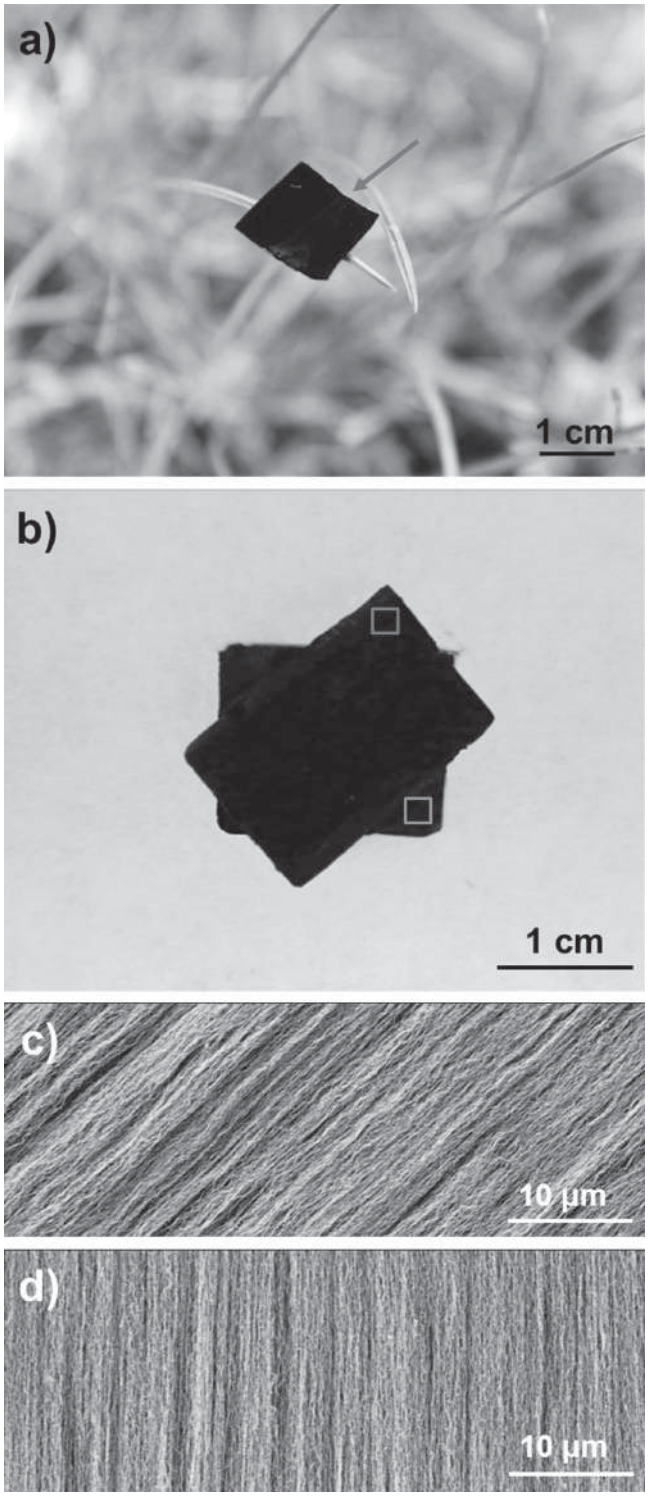

Figure 1. a) Photograph of a lightweight aligned CNT film on a leaf. b) Photograph of two aligned CNT films stacked with an intersectional angle of appropriately 45°. c,d) SEM images of the upper and lower rectangles in (b), respectively.

(Figure 1c,d). Figure S2 in the Supporting Information further exhibits two-dimensional small-angle X-ray scattering patterns that verify the increasing intersectional angles from 0 to 90°.

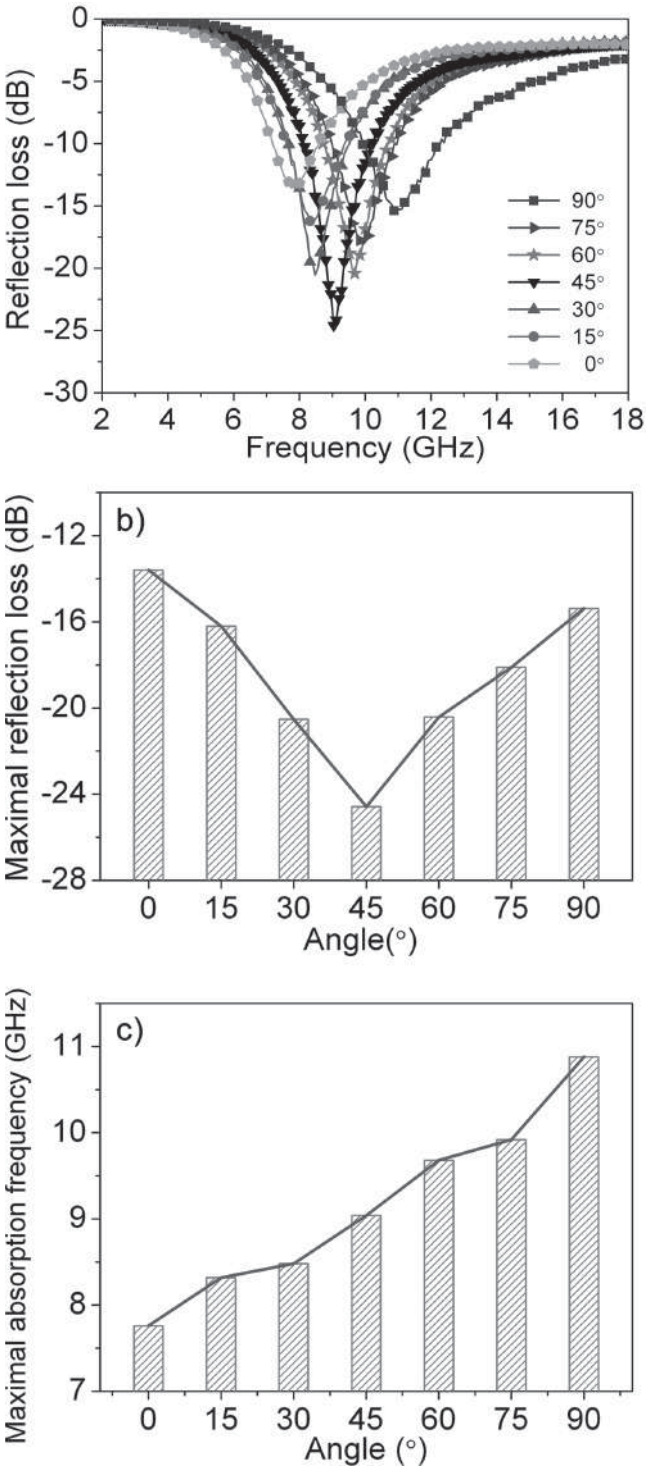

Figure 2. a) Reflection loss curves of two stacked aligned CNT films with intersectional angles of 0, 15°, 30°, 45°, 60°, 75°, and 90° at the same thickness of 2 mm. b,c) Dependence of the maximal reflection loss and absorption frequency on the intersectional angle, respectively.

The above CNT films with the intersectional angle range of 0–90° were compared in the microwave absorption measurement (Figure S3, Supporting Information). **Figure 2**a shows the reflection loss curves of two stacked aligned CNT films. In the

measurements, paraffin was incorporated into the stacked CNT films with the same thickness of 2 mm. The maximal reflection loss value is first increased from −13.60 to −24.58 dB with the increasing intersectional angle from 0 to 45° and then decreased to −15.38 dB upon the further increase to 90° (Figure 2b). Differently, the maximal absorption frequency was increased monotonously from 7.76 to 10.88 GHz with the increasing intersectional angle from 0 to 90° (Figure 2c). To reveal the electric field distribution around the aligned CNTs films with increasing intersectional angles, off-axis electron holography technique was used to map the dielectric potential. The off-axis electron holography was recorded at a biprism voltage of 50 V in vacuum. For the convenience of characterization, aligned CNT films with a lower thickness of ca. 20 nm with intersectional angles of 0, 45, and 90° were studied as a demonstration (Figure S4, Supporting Information). The intersectional angles between two aligned CNT films were observed as designed (Figure S5, Supporting Information). The polarization shapes contributed from their electric fields were sensitively reflected by the off-axis electron holography. The intersectional angle of 45° showed the most dominant isotropic feature, which may be beneficial to the microwave absorption from a viewpoint of polarization (Figure S6, Supporting Information).[27]

To understand the mechanism of the microwave absorption at different intersectional angles, the dependence of the complex permittivity and permeability on frequency was investigated. For all the samples, the real part (μ′) and imaginary part (μ″) of the complex permeability were independent on the frequency in the investigated range, indicating that the aligned CNT films hardly produce any magnetic loss (Figure S7, Supporting Information). **Figure 3**a and 3b show the dependence of real part (ε′) and imaginary part (ε″) of complex permittivity on the frequency. For all samples, the ε′ values were decreased from 2 to 18 GHz with a rapid decrease between 2 and 6 GHz and a relatively slower decrease between 6 and 18 GHz. The ε′ value represents the storage capability of the electric energy inside the absorber, and a lower ε′ value favors a balance between permeability and permittivity, thus decreasing the reflection coeffcient of the absorber. The ε′ values were decreased monotonously with the increasing intersectional angle from 0 to 90°, indicating a decreased storage capability (Figure 3a and Figure S8a, Supporting Information). The ε″ value corresponds to the energy loss caused by the electric dipole moment rearrangement under electric field. For all samples, the ε″ values were decreased with the increasing frequency, and double dielectric resonance peaks appeared at 8.4 and 13.9 GHz (Figure 3b). The ε″ value were rapidly decreased with the increasing intersectional angles from 0 to 60° and then remained almost unchanged with the further increase to 90° (Figure S8b, Supporting Information).

The dielectric loss tangent ($\tan\delta_e = \varepsilon''/\varepsilon'$) is another critical factor to evaluate the microwave absorption performance of an absorber. The higher the tangent value, the more electromagnetic wave energy is converted to the other form of energy, mainly thermal energy. For all samples, the $\tan\delta_e$ values were increased with the increasing frequency from 2 to 14.9 GHz and then reached a platform with the further increase in frequency. The aligned CNT films at the intersectional angle of 0° showed the highest $\tan\delta_e$ value, and the values were decreased

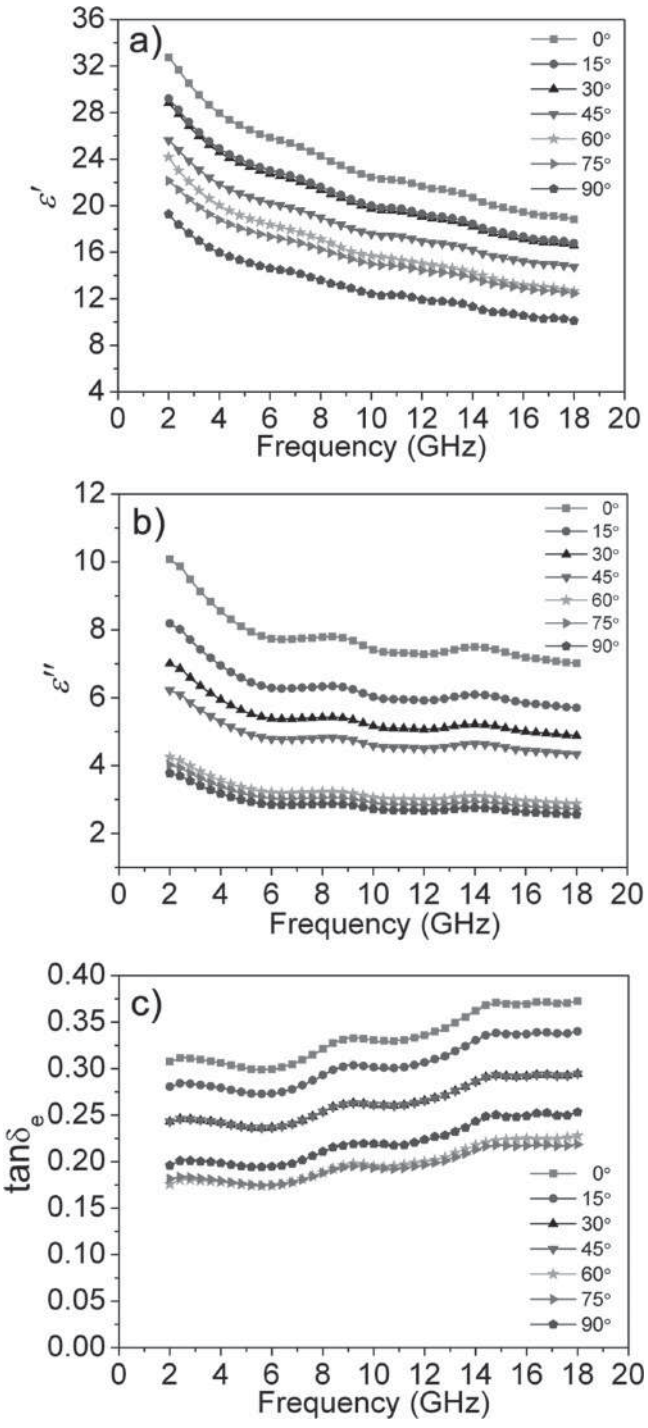

Figure 3. Dependence of real (a) and imaginary parts (b) of the complex permittivity and dielectric loss (c) on frequency for two stacked, aligned CNT films with the intersectional angles of 0, 15°, 30°, 45°, 60°, 75°, and 90° and the same thickness of 2 mm. Here ε′ and ε″ represent the real and imaginary parts of complex permittivity, respectively, and δ_e corresponds to the dielectric loss.

with the increasing intersectional angle, indicating a decreased conversion capability of the electromagnetic wave. Although the $\tan\delta_e$ value at 45° was not the highest, the intersectional angle of 45° showed the best microwave absorption performance,

which may be explained by a balance of two key factors. At low intersectional angles of 0–30°, the high electromagnetic wave conversion capability was derived from a high $\tan\delta_e$, but the reflection coeffcient was also high due to a high ε' value as a lot of electromagnetic wave was reflected back with a low absorption; at high intersectional angles of 60–90°, the reflection of electromagnetic wave was not prominent, but the electromagnetic wave conversion capability was inferior, which also led to a decrease in absorption performance; at 45°, a balance was struck between the reflection and conversion of the electromagnetic wave, and the best absorption performance was achieved as a result.

Basically, the electromagnetic wave is composed of electric and magnetic components being vertical with each other and the propagation direction is determined by the Poynting vector. Herein, the polarization of two CNT sheets generates a composite polarization interacting with the propagated microwave. The unique design changes the composite polarization direction by varying the intersectional angle between two neighboring CNT sheets from 0 to 90 degree. It is spotted that the intersectional angle sensitively affects the polarization coupling between two neighboring CNT sheets and determines its vector when the microwave propagates inside. Therefore, a dependence of absorption frequency on intersectional angle was observed.

It should be noted that the maximal absorption frequency was varied with the increasing intersectional angle. According to Equation 1, a larger value of hyperbolic tangent produces a higher input impendence of the microwave absorption material. The change in frequency may be attributed to the change of the dielectric constant with the increasing intersectional angle as the samples share the same thickness. For conventional microwave absorption materials, the absorption frequency can be only tuned by varying the coating thickness. Here a new strategy is presented to tune the absorption frequency by varying the intersectional angle of aligned nanomaterial films. Compared with the randomly dispersed CNT film, which has an isotropic structure that exhibited much lower maximal reflection loss of –5.9 dB (Figure S9, Supporting Information), the aligned structure had a critical influence on the high performance. In addition, the aligned structure was tunable during the preparation and was important in making a systematical study of the structure–property relationship.

Figure 4a further compares the microwave reflection loss curves of 2, 3 and 4-layered aligned CNT films with the same intersectional angle and thickness of 90° and 2 mm, respectively. With the increasing layer number, the maximal reflection loss was increased from –15.28 to –47.66 dB, and the maximal absorption frequency moved to high-frequency regions from 11.04 to 12.32 GHz. The absorption bandwidth was also increased from 2.32 to 4.4GHz (<–10 dB), indicating a remarkable improvement in microwave absorption.

A second phase can be incorporated into the aligned CNT films to improve the microwave adsorption, and Fe and polyaniline (PANI) were studied as two demonstrations (Figure 4b,c). Figure S10 in the Supporting Information compares the surfaces of the aligned CNT/Fe composite films with different Fe thicknesses of 10 and 100 nm. Fe was first coated on the surfaces of CNTs with increasing diameters and completely

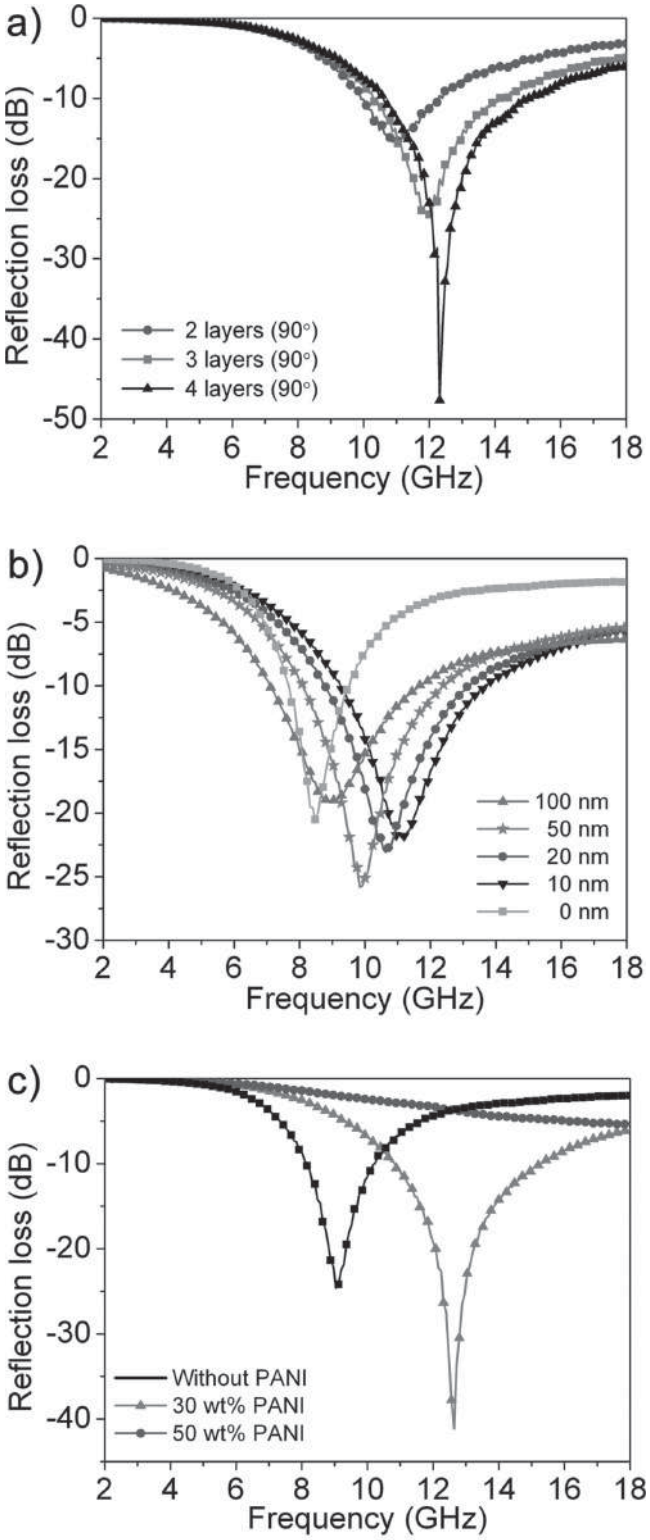

Figure 4. a) Microwave reflection loss curves of 2-, 3-, and 4-layered aligned CNT films with the same intersectional angle and thickness of 90° and 2 mm, respectively. b) Microwave reflection loss curves of aligned CNTs films coated with Fe at different thicknesses of 0, 10, 20, 50, and 100 nm. c) Microwave reflection loss curves of aligned CNTs coated with PANI at different weight percentages of 0, 30, and 50%. All the samples shared the thickness of 2 mm.

covered at the top of the aligned CNT sheet with the formation of nanoparticle (average diameter of ca. 100 nm) (Figure S10). The aligned CNT/Fe composite films were stacked with an intersectional angle of 45°. Figure 4b represents the reflection loss curves of the aligned CNT/Fe films with increasing Fe thicknesses. The maximal reflection loss was increased from –20.53 to –25.83 dB with the increasing thickness from 0 to 50 nm and then decreased to –18.95 dB with the further increase to 100 nm, even lower than the bare aligned CNT sheet. The maximal absorption frequencies first moved to high-frequency regions with the increasing thickness from 0 to 10 nm and then returned to low-frequency regions with the further increase in thicknesses. The absorption bandwidth was increased from 1.84 to 4.32 GHz (<–10 dB) at the Fe thickness from 0 to 10 nm and maintained at ca. 4.4 GHz with the further increase to 100 nm.

PANI was also found to improve the microwave absorption of aligned CNT film. Figure S11 in the Supporting Information shows the surface of the aligned CNT/PANI film with the PANI weight percentage of 30% and a layer of PANI was uniformly coated on the surfaces of CNTs. Figure 4c compares the microwave reflection loss curves of bare aligned CNT and CNT/PANI composite films with PANI weight percentages of 30% and 50%. The intersectional angle and thickness were 45° and 2 mm, respectively. With the incorporation of PANI with a weight percentage of 30%, the maximal reflection loss was increased from –24.58 to 41.14 dB, and the maximal absorption frequency moved from 9.04 to 12.64 GHz. The absorption bandwidth was also increased from 2.04 to 4.43 GHz (<–10 dB). With the increasing PANI weight percentage to 50%, no absorption peaks had been observed.

In conclusion, aligned CNT films were used as light-weight, frequency-tunable and high-performance microwave absorbers. The maximal absorption frequency can be controlled by varying the intersectional angles of aligned CNT films, and the maximum microwave reflection loss can be further increased by increasing the stacked number of aligned CNT films and incorporation of other moieties such as inorganic Fe and organic polymer. These aligned CNT-based films represent a new family of microwave absorption materials.

Experimental Section

Preparation of Aligned CNT Films: Aligned CNT films were prepared from vertically aligned CNT arrays that had been synthesized by chemical vapor deposition.[28] The synthesized CNT arrays exhibited a thickness of ca. 1.5 mm (Figure S1, Supporting Information). A polytetrafluoroethylene roller with a smooth surface was used to press the array down to form the aligned CNT film. The resulting CNT films could be easily peeled off from the substrate by a sharp doctor blade.

Preparation of Aligned CNT/Fe and CNT/PANI Films: Electron-beam evaporation deposition was used to directly deposit Fe onto an aligned CNT film in a DZS-500. The thickness of the Fe layer was determined by a thickness monitor based on a quartz crystal microbalance. To prepare the aligned CNT/PANI films, aligned CNT films were firstly immersed in the electrolyte containing 0.1 M aniline and 1.0 M H_2SO_4 for 4 h to improve the permeation of the monomer into the aligned CNTs, and electro-polymerization of aniline was then performed at 0.75 V vs SCE. The weight of PANI can be calculated from the total Faradic charge consumed during the electropolymerization by assuming an average of 2.5 electrons per monomer.[29,30]

Electromagnetic Measurements: For the aligned CNT films with different intersectional angles, two aligned CNT films were stacked with designed angles and pasted together by commercial glue. The resulting film was cut into narrow ribbons with a dimension of 10 mm by 2.3 mm. The narrow ribbons were further adhered together by the glue, followed by coaxially wrapping onto a rod with a diameter of 3 mm. The multilayered CNT films and aligned CNT/Fe or CNT/PANI composite films were prepared by the same procedure. The 2-, 3-, and 4-layered aligned films had 6, 10, and 13 CNT sheets, respectively. The complex relative permittivity, permeability, and reflection loss were measured between 2 and 18 GHz at a HP8510C vector network analyzer.

Supporting Information

Supporting Information is available from the Wiley Online Library or from the author.

Acknowledgements

This work was supported by MOST (2013CB932901, 2011CB932503), NSFC (21225417, 51172047, 11274066, 51102050, U1330118, and 51132002), STCSM (12nm0503200), the Fok Ying Tong Education Foundation, the Program for Professor of Special Appointment at Shanghai Institutions of Higher Learning, the Program for Outstanding Young Scholars from Organization Department of the CPC Central Committee, and the Pujiang Program and "Shu Guang" project of the Shanghai Municipal Education Commission and the Shanghai Education Development Foundation (09SG01).

Received: August 15, 2014
Revised: September 18, 2014
Published online: October 22, 2014

[1] F. J. Ren, H. J. Yu, L. Wang, M. Saleem, Z. F. Tian, P. F. Ren, *RSC Adv.* **2014**, *4*, 14419–14431.
[2] T. Zhao, C. Hou, H. Zhang, R. Zhu, S. She, J. Wang, T. Li, Z. Liu, B. Wei, *Sci. Rep.* **2014**, *4*. 5619.
[3] K. J. Vinoy, R. M. Jha, *Radar Absorbing Materials: From Theory to Design and Characterization*, Kluwer Academic Publishers, Boston, MA, USA **1996**.
[4] P. Singh, V. K. Babbar, A. Razdan, R. K. Puri, T. C. Goel, *J. Appl. Phys.* **2000**, *87*, 4362–4366.
[5] R. C. Che, L. M. Peng, X. F. Duan, Q. Chen, X. L. Liang, *Adv. Mater.* **2004**, *16*, 401–405.
[6] F. Qin, C. Brosseau, *J. Appl. Phys.* **2012**, *111*. 061301.
[7] J. M. Thomassin, C. Jerome, T. Pardoen, C. Bailly, I. Huynen, C. Detrembleur, *Mater. Sci. Eng., R.* **2013**, *74*, 211–232.
[8] B. Wen, M. S. Cao, M. M. Lu, W. Q. Cao, H. L. Shi, J. Liu, X. X. Wang, H. B. Jin, X. Y. Fang, W. Z. Wang, J. Yuan, *Adv. Mater.* **2014**, *26*, 3484–3489.
[9] H. J. Yang, M. S. Cao, Y. Li, H. L. Shi, Z. L. Hou, X. Y. Fang, H. B. Jin, W. Z. Wang, J. Yuan, *Adv. Optical Mater.* **2014**, *2*, 214–219.
[10] T. Xia, C. Zhang, N. A. Oyler, X. B. Chen, *Adv. Mater.* **2013**, *25*, 6905–6910.
[11] B. Wen, M. S. Cao, Z. L. Hou, W. L. Song, L. Zhang, M. M. Lu, H. B. Jin, X. Y. Fang, W. Z. Wang, J. Yuan, *Carbon* **2013**, *65*, 124–139.
[12] G. Z. Wang, Z. Gao, S. W. Tang, C. Q. Chen, F. F. Duan, S. C. Zhao, S. W. Lin, Y. H. Feng, L. Zhou, Y. Qin, *ACS Nano* **2012**, *6*, 11009–11017.
[13] Y. L. Yang, M. C. Gupta, *Nano Lett.* **2005**, *5*, 2131–2134.

[14] T. H. Ting, Y. N. Jau, R. P. Yu, *Appl. Surf. Sci.* **2012**, *258*, 3184–3190.
[15] K. R. Paton, A. H. Windle, *Carbon* **2008**, *46*, 1935–1941.
[16] H. Sun, Z. B. Yang, X. L. Chen, L. B. Qiu, X. You, P. N. Chen, H. S. Peng, *Angew. Chem. Int. Ed.* **2013**, *52*, 8276–8280.
[17] Z. B. Yang, T. Chen, R. X. He, G. Z. Guan, H. P. Li, L. B. Qiu, H. S. Peng, *Adv. Mater.* **2011**, *23*, 5436–5439.
[18] J. Chen, Y. Liu, A. I. Minett, C. Lynam, J. Z. Wang, G. G. Wallace, *Chem. Mater.* **2007**, *19*, 3595–3597.
[19] A. Gohier, B. Laik, K. H. Kim, J. L. Maurice, J. P. Pereira-Ramos, C. S. Cojocaru, P. T. Van, *Adv. Mater.* **2012**, *24*, 2592–2597.
[20] J. Ren, L. Li, C. Chen, X. L. Chen, Z. B. Cai, L. B. Qiu, Y. G. Wang, X. R. Zhu, H. S. Peng, *Adv. Mater.* **2013**, *25*, 1155–1159.
[21] T. Chen, H. S. Peng, M. Durstock, L. M. Dai, *Sci. Rep.* **2014**, *4*, 3612.
[22] A. B. Dalton, S. Collins, E. Munoz, J. M. Razal, V. H. Ebron, J. P. Ferraris, J. N. Coleman, B. G. Kim, R. H. Baughman, *Nature* **2003**, *423*, 703–703.
[23] H. Sun, X. You, J. Deng, X. Chen, Z. Yang, J. Ren, H. Peng, *Adv. Mater.* **2014**, *26*, 2868–2873.
[24] X. M. Sun, W. Wang, L. B. Qiu, W. H. Guo, Y. L. Yu, H. S. Peng, *Angew. Chem. Int. Ed.* **2012**, *51*, 8520–8524.
[25] C. Wei, L. M. Dai, A. Roy, T. B. Tolle, *J. Am. Chem. Soc.* **2006**, *128*, 1412–1413.
[26] M. E. Roberts, M. C. LeMieux, Z. N. Bao, *ACS Nano* **2009**, *3*, 3287–3293.
[27] J. J. Xu, J. W. Liu, R. C. Che, C. Y. Liang, M. S. Cao, Y. Li, Z. W. Liu, *Nanoscale* **2014**, *6*, 5782–5790.
[28] L. B. Qiu, X. M. Sun, Z. B. Yang, W. H. Guo, H. S. Peng, *Acta Chim. Sinica* **2012**, *70*, 1523–1532.
[29] H. Sun, X. You, J. Deng, X. L. Chen, Z. B. Yang, P. N. Chen, X. Fang, H. S. Peng, *Angew. Chem. Int. Ed.* **2014**, *53*, 6664–6668.
[30] H. J. Lin, L. Li, J. Ren, Z. B. Cai, L. B. Qiu, Z. B. Yang, H. S. Peng, *Sci. Rep.* **2013**, *3*. 1353.